

Case study of intraseasonal convection events during strong positive IOD period based on MJO moisture mode theory

Introduction

The Madden–Julian Oscillation (MJO), as the dominant intraseasonal mode in the tropics, is characterized by statistically coherent and dynamically coupled circulations and convective systems, which can be distinguished as alternating active and inactive phases that propagate eastward. This oscillation can also be seen as a cycle of convection followed by suppressed convection initializing and developing over the western Indian Ocean (WIO), and then propagating eastward across the Eastern Indian Ocean (EIO), the Maritime Continents (MC), and occasionally even the Western Pacific Ocean. Both wet and dry phases are components of the intraseasonal oscillation, but the former tends to be of more interest because the latent heat released in moist convection plays a role in many theories underlying the MJO and its teleconnections. These MJO-related eastward propagating intraseasonal signals of enhanced convection are referred to as MJO events hereafter.

Not all of the active intraseasonal signals initiated over the WIO propagate eastward, as convective systems are also modulated by other multi-scale interactions, including air-sea interactions. Hirata et al. (2013) classified intraseasonal variability over the Indian Ocean into the canonical MJO, an eastward decaying type (ED), and an eastward intensifying type (EI). For a fixed domain, extensive and persistent positive SST anomalies are required to initialize the convective phase, and are critical to determining whether convection over the WIO propagates eastward.

The background field of the Indian Ocean during fall 2019 was distinguished by an extremely strong positive Indian Ocean Dipole (IOD) phase, with the the Dipole Mode Index (DMI) reaches its maximum value over the prior 40 years record (Fig. 1a shows the last five years of the time series). A positive IOD phase corresponds to stronger tropical easterly winds and stronger upwelling in the EIO, resulting in a pattern of warmer SSTs in the WIO and colder SSTs in the EIO, which Webster (2020) suggests is associated with weaker MJO propagation. The positive IOD phase also favors moisture convergence over the WIO but suppresses it south of the equator over the EIO (Fig. 1b). This pattern is primarily favorable for convection initiation over the WIO but not for eastward propagating MJO convective phases that travel over the EIO.

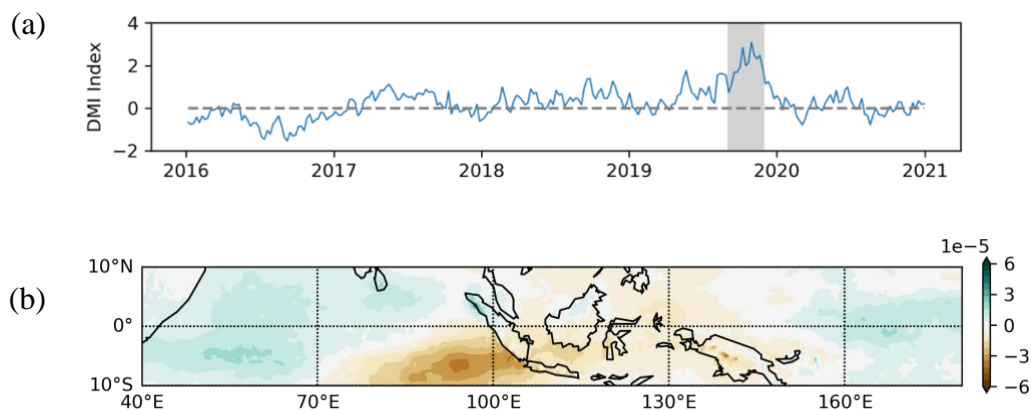


Figure 1 (a) Time series of DMI with the focused period (2019 SON) shaded in grey and (b) regression of column-integrated horizontal moisture convergence onto the DMI index over 1981-2021.

Intraseasonal convection anomalies during the strong positive IOD phase of Fall 2019 can be seen as two events. One occurred around Sep. 20, when convection developed over the central tropical Indian Ocean and then dissipated locally. The other occurred around Oct. 20, when convection initiated over the central tropical Indian Ocean and propagated eastward like a canonical MJO event, evolving through several MJO phases. It is not immediately clear why the first event is more like an ED type while the second event was more like a canonical MJO event, especially with SST and moisture convergence so unfavorable for MJO eastward propagation. In this paper, the composite background fields of both events are examined with the theoretical framework for MJO propagation, and a preliminary qualitative analysis is conducted.

The structure and propagation of the MJO are partly explained by theories of convectively coupled equatorial waves. Moreover, a moist framework that considers the role of moisture asymmetry is required to further explain key features of MJO, such as the propagation speed. Several theories have been proposed, including the moisture mode theory (Zhang et al., 2020). The moisture mode theory emphasizes the role of phase leading moisture anomalies on eastward propagation. Hsu and Li (2012) examined contributors to the phase leading planetary boundary layer (PBL) moisture anomaly by conducting an intraseasonal moisture budget analysis. They concluded that the Ekman pumping due to the Kelvin wave response is the key contributor to generating and maintaining the leading PBL moisture pattern. Hu et al. (2021) further examined two types of the moisture mode theory, one considering the zonal asymmetry of the moist static energy (MSE) tendency as the main reason for propagation, and the other emphasizing the zonal asymmetry of PBL moisture.

Similar composite budget analyses for the two intraseasonal convection events is conducted as a first step in explaining the question raised above. A further decomposition of the advection and radiation terms is used to separate the roles of different physical processes and link the anomalies linked to detailed theories. In this paper, the composite fields of the two events are analyzed and preliminary quantitative results are given for the moisture and MSE budget analyses.

Data and method

To identify the convection centers, the NCEP/NOAA Interpolated Outgoing Longwave Radiation (OLR) dataset (Liebmann & Smith, 1996) is used, along with the principal components and EOF patterns related to MJO, specifically the Filtered OLR MJO index (FMO) (*The Filtered OLR MJO Index and FMO EOF Patterns*, n.d.) from the archive of MJO indices at NOAA Physical Sciences Laboratory (PSL). The ECMWF reanalysis v5 (ERA5, Copernicus Climate Change Service, 2017) is used to construct detailed regressions and composites, including temperature, specific humidity and geopotential height on pressure levels; surface fluxes and vertical-integrated fields from the single-level product, and heating rates and moisture source/sink due to physical parameterizations from the complete product. All of the data and reanalysis products are daily data covering a reasonable period to pick out intraseasonal signals (2019.06-2020.02). The horizontal resolution is $2.5^{\circ} \times 2.5^{\circ}$ for the OLR data and $1^{\circ} \times 1^{\circ}$ for the reanalysis products. For the background state, the weekly DMI time series (*OOPC*, n.d.) from 1981.11 to present is retrieved from the the Ocean Observations Panel for Climate, NOAA and moisture flux convergence from ERA5 is regressed onto it.

It is straightforward to distinguish signals of eastward propagating MJO events on a Hovmöller diagram of OLR anomalies (i.e. a time-longitude plot of meridional mean OLR anomalies). OLR values can be either intraseasonal (20d-70d) bandpass-filtered (Wang et al.,

2019) or reconstructed using the RMM index (e.g., Hu et al., 2021). Although the events of interest in this paper are not canonical MJO events, a similar approach is applied to track intraseasonal convection anomalies and locate the convection centers, based on which the composite mean background fields of both the eastward propagating and stationary events are retrieved.

As shown in Fig. 1, the OLR anomalies reconstructed from the FMO PCs shows clearer and smoother signals compared to the bandpass-filtered signals, and is therefore used for locating the convection centers. However, it should be noted that reconstruction can be viewed as a method for smoothing the signal and FMO is also built on filtered data, so this procedure may result in excessive signal loss. However, FMO is the only index for which both EOFs and PCs can be easily accessed. Reconstruction using the RMM index and other methods for distinguishing intraseasonal variability over the Indian Ocean will be assessed in the further to test whether they can track convective anomalies more accurately.

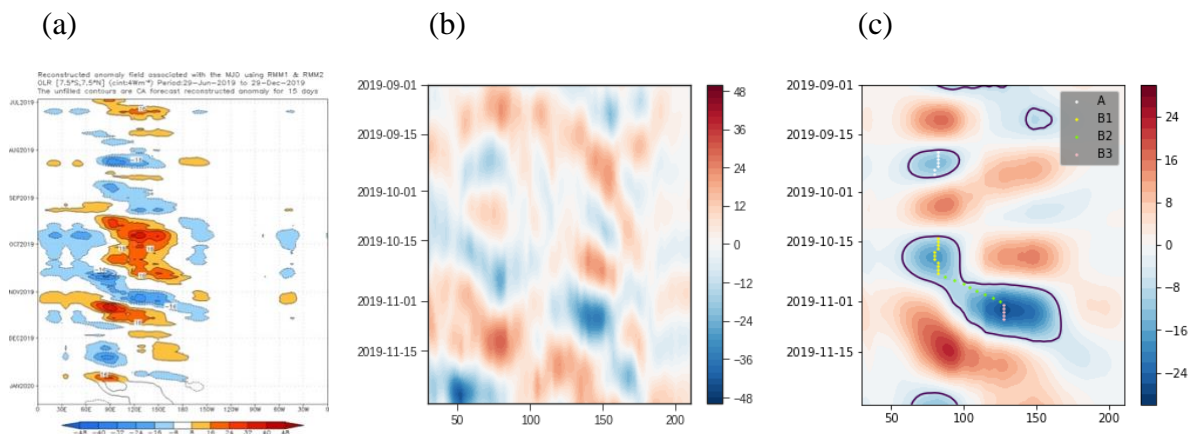


Figure 2 The OLR anomalies reconstructed by RMM1 and RMM2 (a, plot retrieved from Rosencrans, 2019), filtered by a 20-70d bandpass filter (b) and reconstructed from FMO PC1 and PC2 (c). Colored dots in (c) denote convective centers tracked for composite analysis.

Convective phases are identified by adopting zonal mean OLR anomalies between 10°N and 10°S less than -7 Wm^{-2} as the main criteria. Convective centers are then defined as the longitude of the minimum zonal mean OLR anomaly, where the most developed deep convection is embedded in larger convective systems. As the propagating signal is still noisy, the trajectory of the convective center on Hovmöller diagram is smoothed and the final selection are shown in Fig. 1c. It appears that the first event was nearly stationary, while the second event was stationary initially before propagating eastward and intensifying east of the Maritime Continent, which can also be interpreted as a jump. Therefore, the centers of the first event (Group A) and the initial stage of the second event (Group B1) are picked as the location of OLR minimum (around 82.5°E), and the same for the other quasi-stationary stage of the second event (Group B3, at 127.5°E). Propagation centers are also tracked for the migrating composites (Group B2) as a smoothed curve based on OLR minimum. It should be noted that group B3 may not be well defined because there were still weak propagating convective anomalies thereafter, and these details are difficult to be properly tracked through current definition based on the zonal mean OLR minimum.

Before conducting the budget analysis, it is necessary to clarify that the moisture budget used in previous studies is based on Yanai et al. (1973):

$$\frac{\partial q}{\partial t} + \mathbf{v} \cdot \nabla q + \omega \frac{\partial q}{\partial p} = -\frac{Q_2}{L_v},$$

where the apparent moisture source Q_2 , theoretically a sum of condensation and vertical eddy transport, is calculated as a residual. Here for ERA5, the parameterization (or ‘physical’) term of the radiation output is used to calculate the budget, i.e., each term in the heat and moisture budget is a model or reanalysis output rather than a residual. Therefore, it is necessary to check the closure of the heat and moisture equation over the dataset, which can be written as:

$$\begin{aligned} \frac{\partial T}{\partial t} + \mathbf{v} \cdot \nabla T + \omega \frac{\partial T}{\partial p} - \omega \frac{RT}{c_p p} &= \frac{Q_C}{c_p} + \frac{Q_R}{c_p} + \varepsilon_T, \\ \frac{\partial q}{\partial t} + \mathbf{v} \cdot \nabla q + \omega \frac{\partial q}{\partial p} &= (E - P) + \varepsilon_q, \end{aligned}$$

where the terms on the left side of the equations are summarized as dynamical terms and the source/sink terms on the right side can be seen as physical terms. ε_T and ε_q are residuals of heat and moisture budgets, respectively, and should have values close to 0. The physical terms are the sum of all the parameterization processes, and the residuals represent the effect of numerical diffusion and data assimilation. Calculating the apparent moisture source as residual is equivalent to assigning all the error to the physical term. Considering the difficulty to assert a reasonable fraction by which the residual should be assigned to each term, it is not easy to conclude which of the two methods is more accurate. In the following budget analyses (Fig. 6-7), large difference sometimes appears between the physical and Yanai terms, especially for group B3, but at least they always have the same sign.

The budgets are examined for an Eulerian domain over the tropical Indian Ocean (60°E-100°E, 10°N-10°S) both for the PBL (700hPa-1000hPa) and the whole tropospheric column (100hPa-surface). Daily time series and intraseasonal filtered series are shown in Fig. 2. The ratio of the residual variance to the variance of the dynamical term (shown in Table 1) is a simple and straightforward measure of budget closure over the dataset. The moisture residual represents a larger fraction of the moisture budget than the heat residual in the heat budget, especially in the PBL. It is not easy to assert whether such a residual is acceptable, so both the physical moistening rate and apparent moisture source term are examined in the subsequent budget analysis.

	heat		moisture	
	not filtered	filtered	not filtered	filtered
PBL	9.70%	2.89%	19.89%	18.11%
column	4.17%	1.11%	7.63%	3.55%

Table 1. Ratio of the residual variance to the variance of the dynamical term, i.e., $\text{var}(\text{residual})/\text{var}(\text{dynamical})$ for the heat and moisture budgets

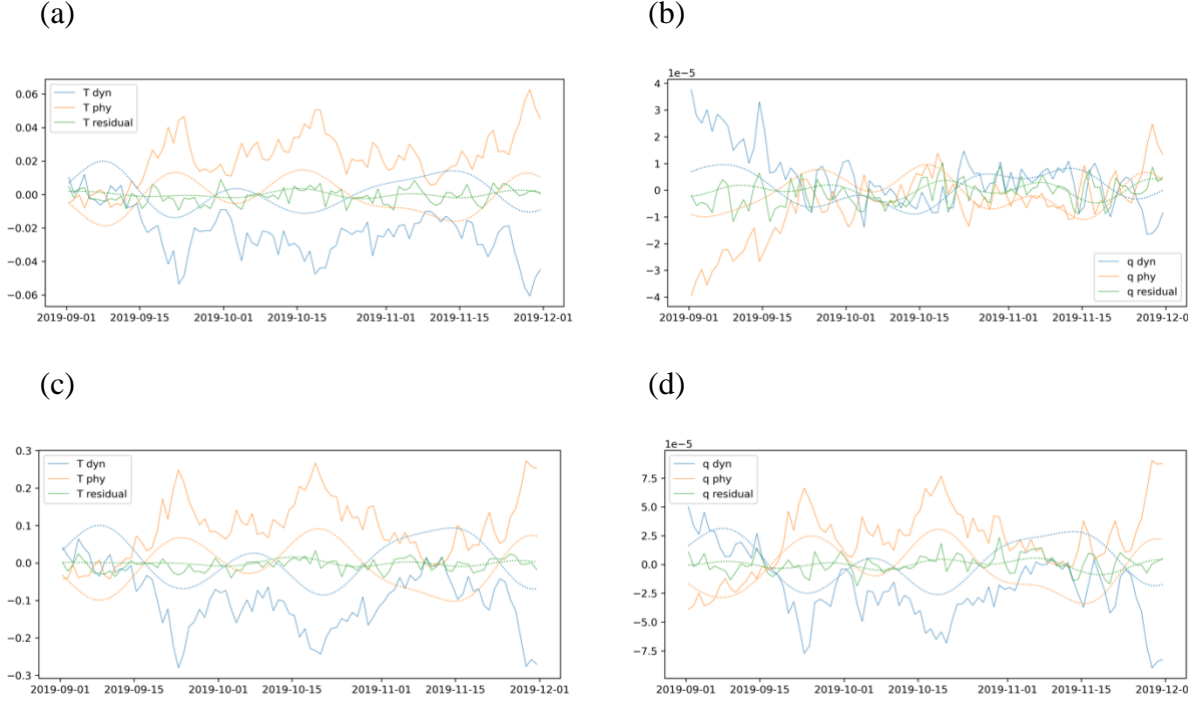


Figure 3 Time series of the dynamical terms, physical terms and residuals in terms of the heat (a, c) and moisture (b, d) budgets integrated over the PBL (a, b) and tropospheric column (c, d) during 2019 SON over tropical Indian Ocean. Solid lines denote unfiltered series and dashed lines denote a 20-70d bandpass filtered series.

Following Hu et al. (2020), the moisture budget in the PBL and the MSE budget integrated for the tropospheric column are examined to determine whether moisture mode theory plays a role in the eastward propagation of the MJO-like event. This framework can be used here to explain why one event propagates while the other does not.

$$\left[\frac{\partial q}{\partial t} \right]' + [\nabla \cdot (\mathbf{v}q)]' + \left[\frac{\partial}{\partial p} (\omega q) \right]' = [E - P]',$$

$$\left\langle \frac{\partial m}{\partial t} \right\rangle' + \langle \nabla \cdot (\mathbf{v}m) \rangle' + \left\langle \frac{\partial}{\partial p} (\omega m) \right\rangle' = Q_R' + Q_{sf c}',$$

Here $[\cdot]$ denotes a mass-weighted vertical integral over the PBL, $\langle \cdot \rangle$ denotes a mass-weighted vertical integrals over the troposphere, and prime denotes the intraseasonal (20-70d bandpass) perturbation. In order to pick out the MJO-related perturbations, both spatial and temporal filtering are required, but spatial filtering is left for further refinement in the future. Each term is computed using daily data, integrated vertically and then finally filtered.

The moisture budget is calculated directly, integrating from 1000hPa to 700hPa. It is worth noting that each term in the MSE budget is calculated as follows and is equivalent to an integral from the surface to the top of atmosphere. Vertical advection term is calculated as the residual of the remaining part of equation, and detailed calculations require interpolation of 3-dimensional data into surface pressure layers, which will be conducted in the near future.

$\left\langle \frac{\partial m}{\partial t} \right\rangle$	Vertical integral of potential, internal and latent energy -> tendency
$\langle \nabla \cdot (\mathbf{v}m) \rangle$	Vertical integral of divergence of total energy flux, vertical integral of divergence of kinetic energy flux
$\left\langle \frac{\partial}{\partial p} (\omega m) \right\rangle$	Residual of the equation
Q_R	tendency of air temperature due to shortwave/longwave heating $\times c_p$ -> vertical intergral
Q_{sfc}	Surface latent/sensible heat flux

Results

Fig. 4-5 shows the composite mean distribution of intraseasonal specific humidity and q tendencies relative to its convective center for each group. Although the previous composite analyses of the MJO-related moisture is based on the budget analysis of the region of positive moisture anomalies, it should be noted that the positive moisture anomalies do not necessarily correspond to a positive moisture tendency. For a propagating convective system with a steady structure, the moisture tendency center will lead the moisture center, possibly be separated from each other in some cases. PBL moisture leading region is defined as $+20^\circ$ to $+50^\circ$ relative to the convective center, the same as is in Hu et al. (2021). As is shown in Fig. 4 there is leading PBL in the propagating group (B2), but no moistening tendency in the same region according to Fig. 5. A moisture tendency leading region is further defined as $+50^\circ$ to $+70^\circ$ relative to the convective center, corresponding to positive PBL moisture tendency specifically in group B2 but there is positive moisture tendencies for all groups.

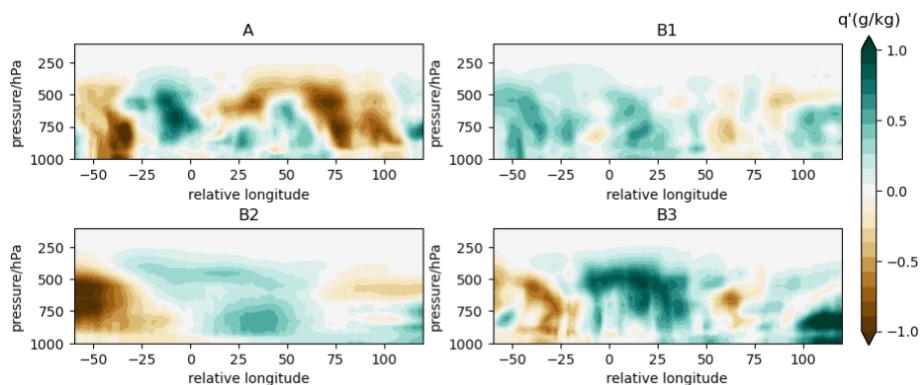


Figure 4 Composite vertical–zonal cross section of intraseasonal specific humidity for groups A, B1, B2 and B3.

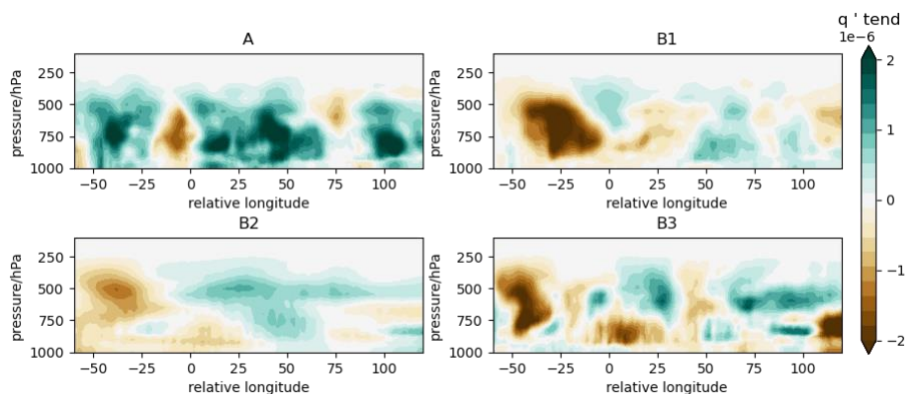


Figure 5 Composite vertical–zonal cross section of intraseasonal specific humidity tendencies for groups A, B1, B2 and B3.

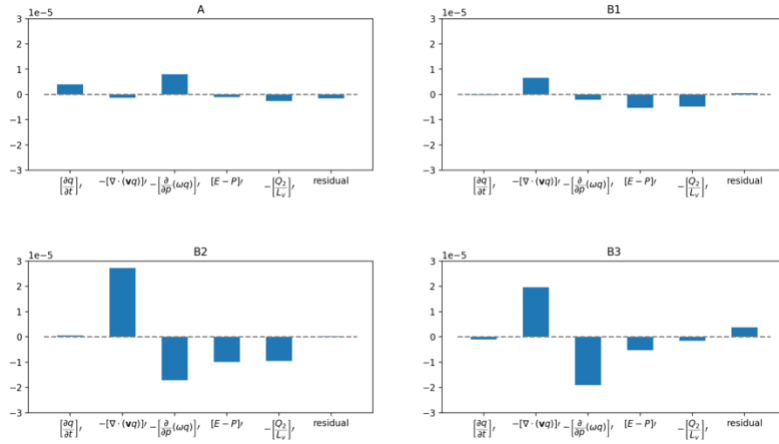


Figure 7. Vertically averaged (1000–700 hPa) moisture budget terms averaged over the moisture leading region of MJO (relative longitude 20°-50°) for groups A, B1, B2 and B3.

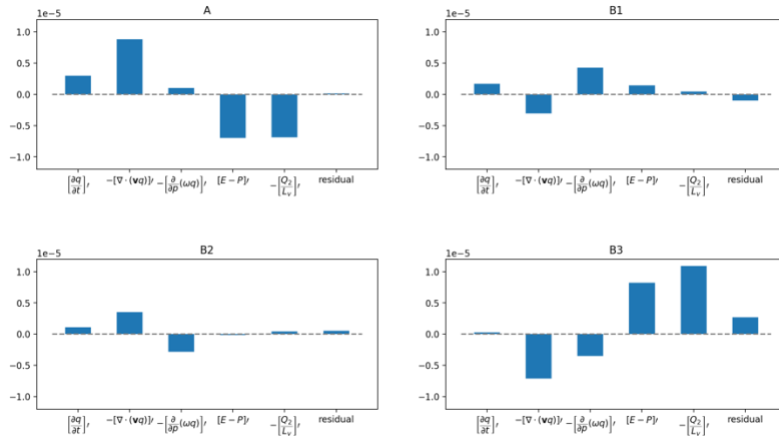


Figure 8 Vertically averaged (1000–700 hPa) moisture budget terms averaged over the moisture tendency leading region of the propagating group (relative longitude 50°-70°) for groups A, B1, B2 and B3.

For the eastward propagating group (B2), an MJO-like structure of moisture is clearly shown with the PBL moisture leading the convective center and mid-troposphere moisture in phase. This pattern is favorable for the upward moisture advection by shallow convection and the subsequent deep convection development, thus resulting in the eastward propagation of convective systems. The PBL moisture leading region was slowly drying during the period of B2. The vertical advection is the major contributor to the negative moisture tendency, indicating that moisture is advected upward from the PBL, consistent with the theoretical picture of shallow convection transporting moisture upward, while the horizontal advection has an opposite contribution to the drying tendency.

Budget analysis over the PBL moisture tendency leading region decomposes the contributions during the initial PBL moistening stage, rather than the moistened stage. It is shown that the horizontal advection contributes to the moisture tendency, partially offset by the vertical advection, and the contribution of the apparent moisture source could be ignored. This partition is quite different from Hsu and Li (2012). This indicates that the physical process of this eastward propagating event deviates from the composite mean of MJO events in terms of moisture mode theory. In addition, the contribution of the horizontal advection term is counter-intuitive because the strong positive IOD is unfavorable for horizontal moisture convergence over MC.

For the quasi-stationary event (group A), the convection initiated in the central tropical Indian Ocean and remained there until dissipation. It is shown that east of the convection center the PBL is moist, while the upper troposphere is dry, but according to Fig. 5, the whole tropospheric column east of the convection center is moistening. Moisture is not advected upward from PBL to the free atmosphere, but increases within both of the two layers. West of the convective center there is a negative moisture tendency for the tropospheric column, which seems to be favorable for the convective system to move eastward, but the convections stay stationary, for which the moisture budget analysis is only for the PBL does not give an explanation.

Group B1 is when the second event initiated in the central tropical Indian Ocean but did not start to propagate eastward. East of the convection center the whole tropospheric column is moist but has a drying tendency in the lower level. So the system did not propagate by means of the development of convection on the eastern side. However, the PBL moisture tendency region is dry but with a moistening tendency, which is far more east and helps the subsequent eastward propagation of the convective system. The propagation can also be described as a jump, as the convective system was weak during propagation and strengthened over the MC. The drying tendency in the PBL moisture leading region is mostly contributed by the physical term. Since there was no intraseasonal convective anomaly over the MC during this period, vertical eddy transport plausibly related to decreased surface evaporation is more likely to be the main contributor than convective condensation. In contrast, the moistening tendency in the PBL moisture tendency leading region (over the eastern MC in this group) is dominated by vertical advection. Similar to what is argued for group A, it is more necessary to conduct a column budget analysis than only for the PBL.

The convective center stayed above the MC and did not propagate further late in the second event (Group B3). As is stated above there is uncertainty in the definition of group B3, so does any conclusion of this section. The upper troposphere is moist from -10° to 30° relative to the convective center, which is possibly the feature of the convective system itself, while there is also a drying tendency from relative longitude 30° to 50° , which is unfavorable for further eastward propagation of convection. Both horizontal and vertical advection contribute to the negative moisture tendency in the PBL in the PBL moisture leading region, but the tendency over the whole tropospheric column needs to be further investigated.

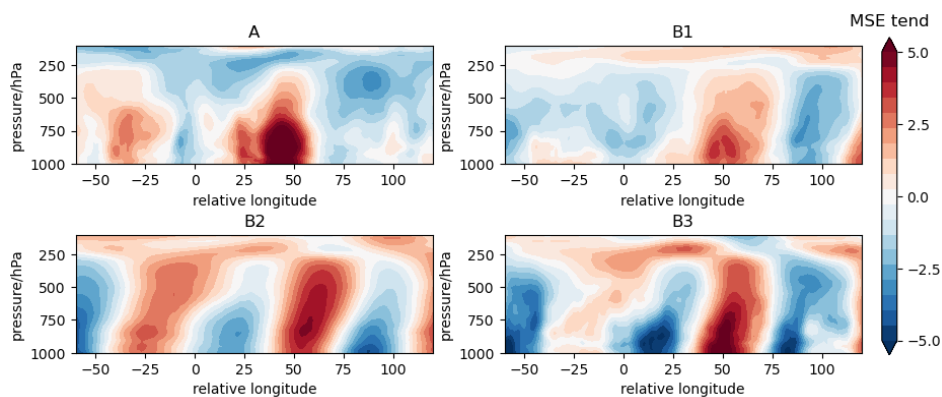


Figure 6 Composite vertical–zonal cross section of intraseasonal MSE tendency for groups A, B1, B2 and B3.

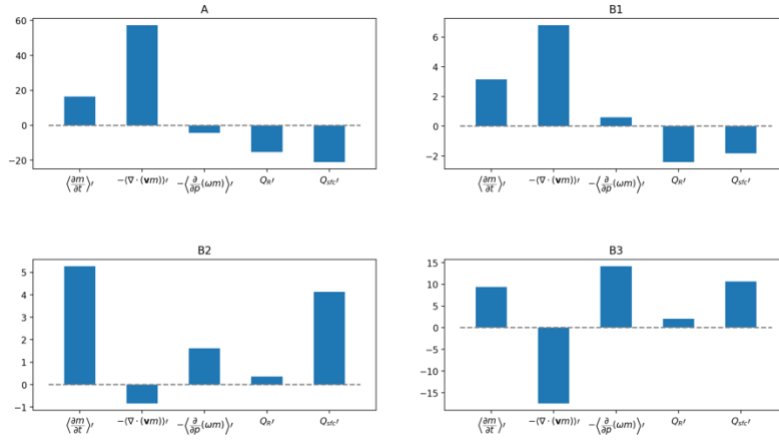


Figure 9 Vertically averaged (surface pressure–100 hPa) MSE budget terms averaged over the MSE tendency leading region MJO (relative longitude 30°–70°) for groups A, B1, B2 and B3.

The MSE composite patterns are zonally asymmetric relative to the convection center. For the propagating group (B2), the positive MSE tendency anomaly on the western side deviates from the composite mean of MJO events. In the MSE tendency leading region (relative longitude 30° to 70°) there are positive anomalies for all of the 4 groups, but the center of anomaly is at the middle troposphere for group B2 and near the PBL for the other groups. From the perspective of the column-integrated MSE tendency, the difference between two events or the four groups is not obvious, so this framework is currently not helpful in explaining the difference between events. The MSE budget analysis is also incomplete because the vertical advection term is still calculated as a residual, but at least it can be concluded that the partition of MSE tendency for group B2 is very different from that in Hu et al. (2021).

Summary and discussions

This study aims to attribute the different evolution of two intraseasonal convection events during the strong positive IOD event in Fall 2019. Although no clear conclusion is addressed from the perspective of the MJO moisture mode theory, there are still many valuable clues.

With the reconstructed OLR anomalies, a stationary event along with the stationary and propagating phases in the other event are defined. Stationary or migrating composite fields of moisture, moisture tendency, and MSE tendency are constructed based on the identified convective centers. Budget analyses are conducted over the region concerned with MJO moisture mode theory. There are preliminary qualitative conclusions for each group, while most of them are negative conclusions. Although the propagating group has a similar moisture distribution as MJO composites, the contributors of moisture tendency are different from that implied by the moisture mode theory, so further explanations for the stationary groups are based on the moisture fields rather than MJO theory. The difference between the initial stationary stage and the propagating stage is moisture tendency east of the convective center, while moisture tendencies far more east may help to set up a background field for the subsequent propagation. The first event may be related to the absence of shallow convection to the east, but this tends to be more of a consequence than a cause. The processes indicated by the moisture budget analysis cannot be considered simply in terms of the IOD influence on moisture advection in different regions. Finally, the difference in column-integrated MSE tendencies between the groups is not obvious.

Methods in this paper still need modifications. The most critical one is that the moisture field is only filtered results rather than anomalies, i.e. the annual cycle is not removed, which

makes it difficult to define anomalous moist and anomalous dry regions. Another noteworthy detail about the data is that the tendency is a centered difference, but the physical tendencies are the average of the previous hour, leading to non-corresponding time steps. This effect is possibly ignored reasonably after the filtering. The identification of the convection centers is also difficult, with the definition of the groups still vague. For example, it is unclear whether the weak propagation after B3 should be classified as another propagation group.

The budget analysis framework is far from perfect. The region to be analyzed should be selected based on the key conclusions from the composite fields, instead of only being limited to PBL. The next step that can be done for the budget analysis is to distinguish the effect of the background field from those of the intraseasonal perturbations. It is also interesting to decompose the cloud radiative effect and further investigate the modulation of the sea-air flux by the IOD and how the flux responses influence MJO. But since the MSE composite fields do not seem to be able to distinguish between propagating and non-propagating events, other frameworks related to heat need to be considered.

There are still many interesting but unexplained phenomena, such as the tilt structure of the MSE tendencies and anomalous positive MSE tendencies on the western side of the convection. Physical terms and Yanai terms in moisture budget analysis seem to have the largest difference over the MC, probably because the assimilation increments are larger over lands, but the reason behind this is still unclear to me.

The effect of the SST pattern of the strong IOD is only slightly mentioned in terms of moisture flux convergence. Many other important effects, such as surface fluxes, are not explored. The role of this effect on the events of interest may be explained by the MJO theories related to WISHE feedback (e.g., Emanuel, 2020), and Webster's qualitative explanations could also be examined, possibly start from calculating contributors to CAPE, but these are very preliminary ideas.

It is also incomplete to consider these events only in terms of MJO-related theories since the eastward propagating signals of MJO are most pronounced during boreal winter. In September and October, the MJO propagation has a non-negligible northward component, referred to as BSISO, and these two months are often not chosen to study its eastward propagation. The frameworks in this paper are zonal mean, without the effects of any meridional asymmetry. But the effects of IOD, at least in terms of the moisture flux divergence, have some meridional asymmetry across the equator. Future progresses should also consider this meridional asymmetry.

References

- Copernicus Climate Change Service (C3S). (2017). *ERA5: Fifth generation of ECMWF atmospheric reanalyses of the global climate*. Copernicus Climate Change Service Climate Data Store (CDS); 2021. <https://cds.climate.copernicus.eu/cdsapp#!/home>
- Emanuel, K. (2020). Slow Modes of the Equatorial Waveguide. *Journal of the Atmospheric Sciences*, 77(5), 1575–1582. <https://doi.org/10.1175/JAS-D-19-0281.1>
- Hirata, F. E., Webster, P. J., & Toma, V. E. (2013). Distinct manifestations of austral summer tropical intraseasonal oscillations: TROPICAL INTRASEASONAL OSCILLATIONS. *Geophysical Research Letters*, 40(12), 3337–3341. <https://doi.org/10.1002/grl.50632>
- Hsu, P., & Li, T. (2012). Role of the Boundary Layer Moisture Asymmetry in Causing the Eastward Propagation of the Madden–Julian Oscillation*. *Journal of Climate*, 25(14), 4914–4931. <https://doi.org/10.1175/JCLI-D-11-00310.1>

- Hu, F., Li, T., Gao, J., & Hao, L. (2021). Reexamining the Moisture Mode Theories of the Madden–Julian Oscillation Based on Observational Analyses. *Journal of Climate*, 34(2), 839–853. <https://doi.org/10.1175/JCLI-D-20-0441.1>
- Liebmann, B., & Smith, C. A. (1996). Description of a Complete (Interpolated) Outgoing Longwave Radiation Dataset. *Bulletin of the American Meteorological Society*, 77(6), 1275–1277. <https://www.jstor.org/stable/26233278>
- OOPC | State of the ocean climate | Surface indices | Indian | DMI. (n.d.). Retrieved June 11, 2021, from <https://stateoftheocean.osmc.noaa.gov/sur/ind/dmi.php>
- Rosencrans, M. (2019). *Madden-Julian Oscillation: Recent Evolution, Current Status and Predictions*. 14.
- The Filtered OLR MJO index and FMO EOF patterns*. (n.d.). 2021. <https://psl.noaa.gov/mjo/mjoindex/#spatial>
- Wang, B., Chen, G., & Liu, F. (2019). Diversity of the Madden-Julian Oscillation. *SCIENCE ADVANCES*, 9.
- Webster, P. (2020). *Dynamics of The Tropical Atmosphere and Oceans* (1st ed.). Wiley. <https://doi.org/10.1002/9781118648469>
- Yanai, M., Esbensen, S., & Chu, J.-H. (1973). Determination of Bulk Properties of Tropical Cloud Clusters from Large-Scale Heat and Moisture Budgets. *Journal of the Atmospheric Sciences*, 30(4), 611–627. [https://doi.org/10.1175/1520-0469\(1973\)030<0611:DOBPOT>2.0.CO;2](https://doi.org/10.1175/1520-0469(1973)030<0611:DOBPOT>2.0.CO;2)
- Zhang, C., Adames, Á. F., Khouider, B., Wang, B., & Yang, D. (2020). Four Theories of the Madden-Julian Oscillation. *Reviews of Geophysics*, 58(3). <https://doi.org/10.1029/2019RG000685>